19

Experimental implementation of a spectral refractive index sensor based on a reflection interferometer

© V.S. Terentyev, V.A. Simonov

Institute of Automation and Electrometry, Siberian BranchRussian Academy of Sciences,
630090 Novosibirsk, Russia

e-mail: terentyev@iae.nsk.su

Received June 7, 2022
Revised June 7, 2022
Accepted October 5, 2022

Experimental study of the sensor in the Kretschmann optical scheme, in which the sensitive element is a reflection interferometer (RI) for the oblique incidence of light, is presented for the first time. A brief theory of RI is given. The experimental sample was used to measure the refractive index of the residual atmosphere in a vacuum chamber during its pumping. The high Q-factor of the RI resonator made it possible to obtain a fairly narrow spectral maximum with a width of 1.7 nm. The spectral sensitivity of the sensor was 1000 nm/RIU and the quality parameter was $529\,\mathrm{RIU}^{-1}$, it was also demonstrated that resolution of $6.5 \cdot 10^{-8}$ RIU can be achieved. Proposals for further improvement of the sensor characteristics are formulated.

Keywords: reflection interferometer, total internal reflection, refractive index sensor.

DOI: 10.21883/EOS.2022.12.55253.3780-22

1. Introduction

Sensors based on the effect of frustrated total internal reflection (FTIR) are used for the study of biomolecular interactions, detection of biological, chemical analytes and in other applications [1]. Sensors based on the Kretschman scheme, in which the probing radiation is coupled to the sensitive layer through a prism, are one of the variants of the FTIR sensors and are most often used in practice. The Kretschman's scheme is bulk with all the disadvantages that follow from this (massiveness of the structure, temperature and vibration instability). These parasitic effects are significantly less susceptible to fiber/waveguide sensors, which are currently actively developing [2]. However, among the advantages of Kretschman's bulk scheme is its lower technological complexity compared to fiber. Assuming the basic principles of the functioning of sensors in the volumetric and fiber versions are the same, the study of the bulk type of sensor based on the FTIR is carried out in order to further optimize the implementation of this sensor in the fiber version.

Sensors based on the Kretschman scheme can be divided into two types. These are, firstly, standard schemes in which the signal reference point is the spectral (or angular) minimum intensity of reflected light generated by absorption during plasmon resonance in the sensitive layer. Secondly, schemes where the reference point is the maximum intensity resulting from a decrease in absorption in the sensor structure. In literature, the latter type of sensors is called inverted [3,4]. In this paper, the second type of sensors is investigated and the possibility of obtaining ultra-high characteristics using the reflection interferometer (RI) method is experimentally demonstrated [5,6]. The method allows the sensor to be manufactured using the standard technology of multilayer dielectric coatings and base metal.

The main objectives of this work are experimental verification of theoretical assumptions and evaluation of the characteristics of the proposed method for sensor applications.

2. RI theory for inclined light incidence

Fig. 1 shows the structure of the sensor under study. It consists of a Prism, a substrate with a refractive index of n_s, a metal layer (Me) with a complex refractive index of n_{Me} deposited on the face of the substrate, and a dielectric multilayer coating based on two materials — with high (for example, TiO_2) and low (SiO_2) refractive coefficients. In this case, the layers adjacent to the metal film go in pairs, alternating with each other, and thus form an RI front mirror M_1, which has a reflection coefficient of R_1 on the side of the substrate and R_2 — on the reverse side facing the base layer (Base). The base layer with a refractive index of n_b determines the free spectral range of RI, and also forms a highly reflective mirror M_2 with a reflection coefficient of R_3 at the boundary of the base and the analyzed medium (Analyte) with a refractive index n_a. A more general theory of RI as applied to this problem can be found in [5]. We give formulas describing the reflection coefficient R of such a system under conditions when the angle of incidence is greater than the FTIR angle ($\sin\theta_b > n_a \sin\theta_b / n_b$) for Base —Analyte media, i.e. when $R_3 = 1$:

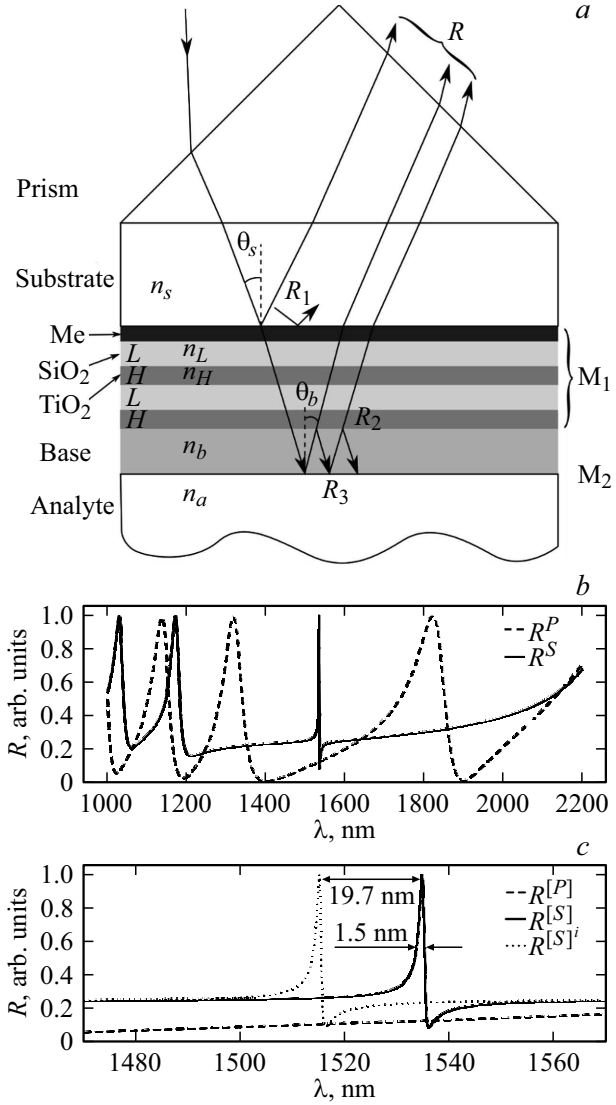

Figure 1. *a* — Kretschmann optical scheme based on RI: Prism — prism, Substrate — plane-parallel substrate, Me — metal thin film, L, H — layers of dielectrics with low and high refractive index, respectively, Base — RI base layer, Analyte — analytical medium, M_1, M_2 — front and rear mirror RI, R_1, R_2 — reflection coefficients M_1, $R_3 = 1$ — mirror reflection coefficient M_2 (interface); *b* — design base reflection coefficients RI for two polarizations $R^{[S]}$ and $R^{[P]}$ in a wide spectral range; *c* — the same, but in a narrow spectral range, the dotted line shows the spectral rearrangement of the maximum $R^{[S]'}$.

$$R(\varphi) = R_1 + 2T_1\sqrt{R_1}\frac{\cos(\vartheta + 2\varphi) - \sqrt{R_2}\cos(\vartheta)}{1 + R_2 - 2\cos(2\varphi)\sqrt{R_2}} + \frac{T_1^2}{1 + R_2 - 2\cos(2\varphi)\sqrt{R_2}}, \quad (1)$$

$$\vartheta = \Psi_1 + \Psi_2 - 2\Phi_1,$$

$$\varphi(\theta_b, \lambda) = \frac{2\pi n_b h_b \cos\theta_b}{\lambda} - \frac{\Psi_2(\theta_b, \lambda) + \Psi_3(\theta_b, \lambda)}{2}, \quad (2)$$

where λ — wavelength, θ_b — angle of light incidence on mirrors inside the resonator, i.e. in the base layer, h_b — physical thickness, n_b — refractive index of the base RI, $R_{1,2}$, $T_1 = T_2$ — energy reflection coefficients of the mirror M_1, $\Psi_{1,2}$ and $\Phi_1 = \Phi_2$ — their phases respectively, R_3, Ψ_3 — the same is true for the mirror M_2. The ratio (1) for $R(\varphi)$ is valid for *S*- and *P*-polarizations with substitution of the corresponding coefficients $R_{1,2}$, T_1 and their phases for these polarizations. In conditions of total internal reflection at the boundary of the base and analyte, the dependence on the parameters of the mirror M_2 is manifested only through the Fresnel phase $\Psi_3(\theta, \lambda)$ in (2), which depends on the refractive index of the analyte n_a.

When using an absorbing metal film in the structure M_1, the reflection coefficients $R_1 \neq R_2$. In the case of quarter-wave dielectric layers for oblique incidence, i.e. when the physical thickness of the dielectric layers is $h_j = \lambda_0/(4n_j\cos\theta_j)$, $j = L, H$, where L — dielectric index with low refractive index, H — with high, λ_0 — central wavelength, $n_L < n_H$, θ_j — the angle of incidence in the jth layer, it is possible to analytically express the energy coefficients of the mirror M_1 for two orthogonal linear polarizations (notation $[S, P]$):

$$R_1^{[S,P]} = \frac{(u_s - \xi_1 - u_b(u_L/u_H)^{2N})^2 + \xi_2^2}{(u_s + \xi_1 + u_b(u_L/u_H)^{2N})^2 + \xi_2^2}, \quad (3)$$

$$R_2^{[S,P]} = \frac{(u_s + \xi_1 - u_b(u_L/u_H)^{2N})^2 + \xi_2^2}{(u_s + \xi_1 + u_b(u_L/u_H)^{2N})^2 + \xi_2^2}, \quad (4)$$

$$T_1^{[S,P]} = T_2^{[S,P]} = \frac{4(u_L/u_H)^{2N}u_s u_b}{(u_s + \xi_1 + u_b(u_L/u_H)^{2N})^2 + \xi_2^2}, \quad (5)$$

where $2N$ — the number of dielectric layers of the mirror M_1, $\xi^{[S,P]} = \xi_1^{[S,P]} + i\xi_2^{[S,P]}$, which are expressed in terms of the thickness of the metal film h_m and its complex refractive index $n_{\mathrm{Me}} = n_m - i\chi_m$:

$$\xi^{[S]} = 2kh_m n_m\chi_m + ikh_m\left((n_m^2 - \chi_m^2) - n_s^2\sin^2(\theta_s)\right),$$

$$\xi^{[P]} = 2kh_m n_m\chi_m + ikh_m(n_m^2 - \chi_m^2), \quad (6)$$

$$u_j = \begin{cases} u_j^{[S]} = n_j\cos\theta_j \ (S \text{ — polarization}), \\ u_j^{[P]} = n_j/cos\theta_j \ (P \text{ — polarization}), \end{cases} \quad (7)$$

$j = s, L, H$. From (3)–(6) it follows that for $u_s = \xi_1$, ones can get $R_1 \ll R_2$ and in the formula (1) only the third term remains significant, which is proportional up to the constant of the transmission function of the Fabry-Perot interferometer. We note that $u_L^{[S]}/u_H^{[S]} < u_L^{[P]}/u_H^{[P]}$ and therefore $R_2^{[S]} > R_2^{[P]}$, i.e. the Q-factor of the resonator for *S*-polarization will be higher than for *P*. For this reason, the maxima for *S*-polarization will be much narrower and more suitable for high-precision measurements of the refractive index of the analyzed medium, although at the same time $d\Psi_3^{[S]}/dn_a < d\Psi_3^{[P]}/dn_a$.

It is possible to determine the main characteristics of the sensor. Finess of the $F^{[S,P]}$ interferometer bands:

$$F^{[S,P]} = \pi \frac{R_2^{[S,P]^{1/4}}}{1 - R_2^{[S,P]^{1/2}}}. \quad (8)$$

The free spectral range of the interferometer:

$$\Delta\lambda \approx \frac{\lambda_0^2}{2n_b h_b \cos\theta_b}\,[\text{nm}]. \quad (9)$$

Spectral width $\delta\lambda$ of intensity maxima:

$$\delta\lambda^{[S,P]} = \frac{\Delta\lambda}{F^{[S,P]}}\,[\text{nm}]. \quad (10)$$

Spectral sensitivities $S_\lambda^{[S,P]}$ are expressed in terms of phase change $\Psi_3^{[S]}$:

$$S_\lambda^{[S]} \approx -\frac{\Delta\lambda}{2\pi}\frac{\partial\Psi_3^{[S]}}{\partial n_a} = \frac{\Delta\lambda}{\pi}\frac{n_a\sqrt{f_b}}{n_b^2 - n_a^2}\frac{1}{\sqrt{f_a}}\,[\text{nm/RIU}], \quad (11)$$

$$S_\lambda^{[P]} \approx -\frac{\Delta\lambda}{2\pi}\frac{\partial\Psi_3^{[P]}}{\partial n_a} = \frac{\Delta\lambda}{\pi}\frac{n_b^2 n_a\sqrt{f_b}}{(n_a^4 f_b + n_b^4 f_a)}\frac{1}{\sqrt{f_a}}\,[\text{nm/RIU}],$$

where $f_a = (n_s \sin\theta_s)^2 - n_a^2$, $f_b = n_b^2 - (n_s \sin\theta_s)^2$.

The sensor quality parameter FOM (Figure of Merit):

$$\text{FOM} = C_R \frac{S_\lambda}{\delta\lambda} = C_R \frac{\Delta\lambda}{\pi\delta\lambda}\frac{d\varphi}{dn_a}, \quad (12)$$

where $C_R = 1 - R_{\min}/R_{\max}$ — contrast of the interference pattern.

Fig. 1, *b* shows the design base reflection spectrum of two polarizations for the parameters corresponding to the experimental ones: $\lambda_0 = 1550$ nm, $h_m = 11$ nm, $n_{\text{Me}} = 3.44{-}6.74i$ RIU (Ni @ 1550 nm), $n_L = 1.46$, $n_H = n_b = 2.4$ RIU, $L = 371.9$ nm, $H = h_b = 178.3$ nm, $N = 4$, $n_s = 1.57$ RIU, $n_a = 1.02$ RIU, $\theta_b = 40.7^\circ$ in a wide spectral range. In Fig. 1, *c*, the dotted line shows the peak offset when $dn_a = -0.02$ RIU changes, which corresponds to a shift of 19.7 nm or sensitivity of 985 nm/RIU. The sensitivity of the sensor depends on the angle of incidence, and the closer to the TIR angle, the higher it is (since it increases $d\Psi_3^{[S,P]}/dn_a$).

3. Experimental setup

For the experimental study, an optical circuit was assembled, including a quartz rectangular prism, a substrate made of BK10 glass, conjugated with a prism using an immersion liquid (glycerin). A sensitive structure was applied to the face of the substrate by magnetron sputtering using the VSE-PVD-100-2 installation (Vacuum systems and electronics), consisting of a thin nickel film, four pairs of dielectric layers SiO_2 and TiO_2 and a base layer of TiO_2. The thicknesses of the dielectric layers were chosen taking into account the multiplier $1/cos\theta_{L,H}$. Thus, in this structure

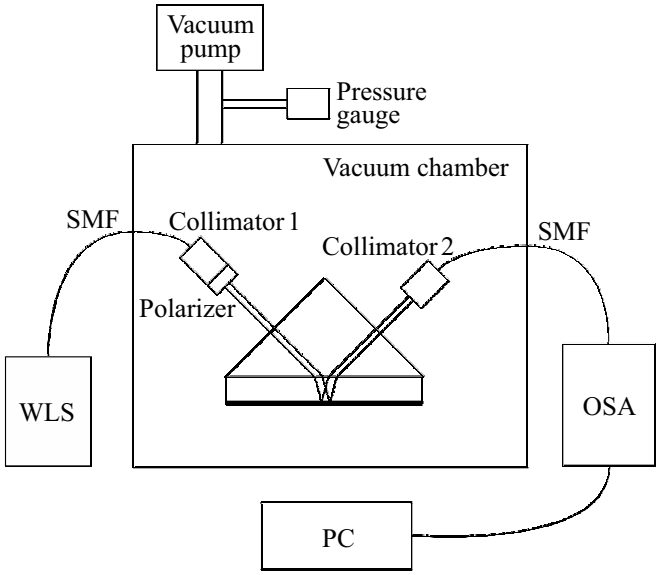

Figure 2. Experimental setup: WLS — white light source, SMF — single-mode fiber type SMF-28e, Collimator *1, 2* — fiber collimators, Polarizer — polarizer, OSA — optical fiber spectroanalyzer, PC — computer, Vacuum chamber — vacuum chamber, Vacuum pump — pre-vacuum pump, Pressure gauge — pressure meter.

there were not quarter-wave layers for normal incidence. The optical control method was not used in the manufacture of the structure, the layers were applied according to time stamps, i.e. the application rate was previously determined by measuring the thickness of the reference layer using the XE15 atomic force microscope (Park Systems). The metal was sputtered at a buffer gas pressure of (Ar) $1.5 \cdot 10^{-3}$ Torr in the voltage stabilization regime of 1 kV and a current of 0.3 A, while for 4 s, the voltage was applied to the magnetron by pulses with a frequency of 27 kHz and a fill factor 10%. When sputtering the dielectric layers, a mixture of gases Ar (75%) + O_2 (25%) $3.6 \cdot 10^{-3}$ Torr was used, voltage — 1 kV; TiO_2: current — 1.57 A, time — 262 s/layer; SiO_2: current — 1 A, time — 200 s/layer, with a frequency of 100 kHz and a fill factor of 36%.

As is known, the refractive index of air with a high degree is linearly proportional to pressure according to the law $n_a(p) = n_{a0} - cp$ at pressures less than atmospheric [7], where $n_{a0} = 1.0002926$ RIU, $c = 2.8 \cdot 10^{-9}$ RIU/Pa, p — pressure. There are optical methods for measuring pressure — for example, based on a change in the phase shift in interferometers due to a change in the refractive index [8,9]. A similar method of optical control was used in this work, but on the basis of the sensor under study.

To determine the main characteristics of the sensor, the circuit shown in Fig. 2 was assembled. As an illuminator (WLS), a broadband white light source FYLA SCT1000 was used (a source of a supercontinuum of 470–2400 nm, pulse duration < 200 ps), the radiation of which was coupled to a single-mode fiber of the SMF-28e type (SMF), the

cut-off wavelength of the higher modes of which 1260 nm. Then the light was collimated using Collimator 1 (Thorlabs F220FC-1550), passed through the Polarizer (Thorlabs LP-NIR050), prism and substrate, reflected from the sensitive layer and coupled to SMF using Collimator 2 (Thorlabs PAF-7-X-C). The spectrum of the reflected signal was measured by an OSA fiber spectrum analyzer (Yokogawa AQ6370) and stored automatically on a computer (PC). To check the sensor response, the atmosphere was pumped out of the chamber using an oil-free forevacuum spiral pump Vacuum pump (Anest Iwata ISP-250C). The pressure in the chamber was controlled using a Pressure gauge (Granvill Phillips 275 Mini-Convectron).

4. Experimental results

Fig. 3, *a* shows the reflection spectrum normalized for reflection from the prism face for *S*-polarization in a wide spectral range with a resolution of 2 nm. As can be seen, there is a very narrow peak in the region of about 1290 nm, comparable to the width of the fiber Bragg lattice. The peak shape is asymmetric and has a side minimum in the long-wavelength region, which corresponds to the design base dependence (Fig. 1, *c*) and is characteristic of the properties of a nickel film. The expected position of the signal maximum is very different from the calculated one (the difference is more than 200 nm). Such a strong spectral shift cannot be obtained solely due to the angle of incidence in the substrate, but together with a shorter base it is quite possible. The peak offset can also be affected by non-standard reflection phases of mirrors M_1 and M_2 ($\Psi_2, \Psi_3 \neq \pi$) due to losses in the multilayer structure. However, most likely the reason is the incorrect determination of the thicknesses of the layers associated with the complexity of obtaining a step of the support layer material on the substrate — i.e. an interference coating designed for a different, shorter wavelength was applied. The rate of sputtering the quarter-wave layer was checked by optical methods and it turned out that the rate was overestimated by about 10% for the SiO_2 layers, however, the rate was determined correctly for TiO_2. The latter means that the thickness of the base layer was applied as expected in the calculation. In any case, modeling of possible errors in the thickness of the layers, i.e. their deviation from the above quarter-wave thickness for oblique incidence, showed that for the materials used, even with an error of about 10% in thickness, a mirror M_1 with a high reflection coefficient from the base can still be formed (R_2), but with the maximum reflection already at a different wavelength.

In Fig. 3, *b*, the signal maximum is shown with a resolution of 1 nm, its spectral width at the level of half the intensity between the minimum and maximum values was $\delta\lambda = 1.7$ nm. The spectral position of the maximum was controlled by searching for the maximum $\lambda_{\max}$ of the approximation polynomial of the third degree (the dashed line in Fig. 3, *b*, almost coinciding with the solid line) according to the intensity level of its spectral width in the spectral range 6 nm. The receiving time of one spectrum was relatively long and was about 30 s, that is, an almost important part of the maximum spectrum accounted for 9 s. This is due to the low level of the reflected signal due to the losses on the insertion into a single-mode fiber at the prism output and, as a consequence, the need to set the OSA high sensitivity mode. In other measurement schemes, for example, based on an inclined spectral filter, the measurement time can be reduced by orders of magnitude [10].

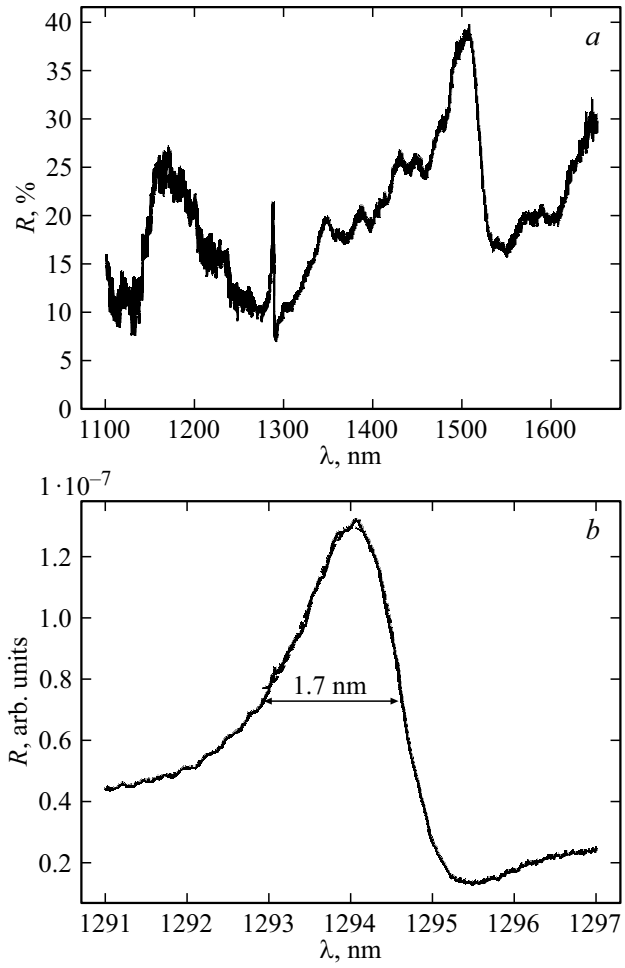

Figure 3. *a* — experimental reflection spectrum in a wide spectral range; *b* — the same in the spectral region of the sensor peak, dashed line — approximation polynomial of the third degree.

Fig. 4, *a* shows the dependence of the wavelength of the maximum $\lambda_{\max}$ on the time in the vacuum chamber during the letting-to-air. The pressure in the vacuum chamber was pumped out to a value of 0.7–0.8 mm Hg (100 Pa). Then, through an external valve, a stepwise letting-to-air with intermediate pressures up to the atmosphere was carried out. At each pressure, the spectra were measured for 5–7 min, which corresponds to 10–15 points on each step. During the measurement at the step $\lambda_{\max}$ was constantly increasing,

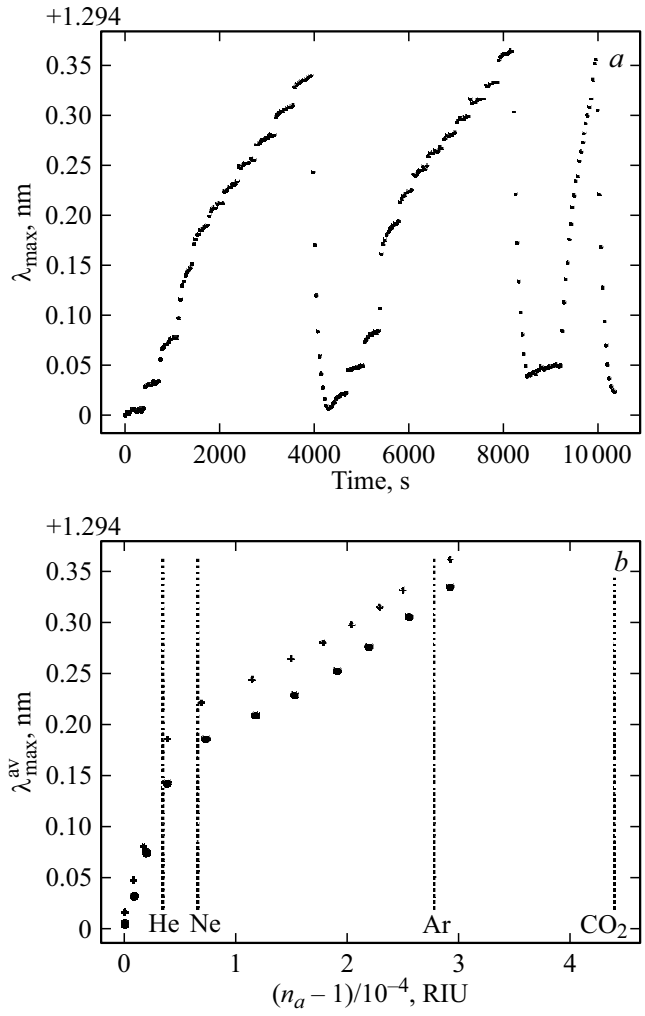

Figure 4. *a* — the dependence of λ_{max} on time; *b* — dependence of λ^{av}_{max} on the change in the refractive index $(n_a - 1)$, circles — the first letting-to-air cycle, crosses — the second letting-to-air cycle, dotted lines show the refractive coefficients of several gases.

which, apparently, was due to the slow heating of the sample due to the lack of thermal stabilization. At the same time, for each step, the pressure gauge reading changed by approximately 1% from the initial value in the decreasing direction. During the letting-to-air into the volume, a thermocouple located inside the vacuum chamber, but at a distance from the sensor, showed a temperature change from 21.6°C at full pumping to 25°C during the letting-to-air. As can be seen from the figure, several pumping and letting-to-air cycles were performed. A stepwise letting-to-air was made twice, rapid pumping was carried out three times and a rapid letting-to-air was carried out once.

According to the data of two-step letting-to-air cycles, the average wavelength λ^{av}_{max} was calculated within each stage and compared with the refractive index calculated from the measured pressure. Fig. 4, *b* shows the dependence of λ^{av}_{max} (from $n_a - 1$), where circles show the first cycle, and crosses — the second. It can be seen that the dependencies are repeated with good accuracy, but they are shifted vertically, which is probably due to the lack of thermal compensation. In addition, the dependencies have a break of about 0.05 RIU, which may be due, for example, to the non-linearity of the response of the pressure meter (insufficient compensation for non-linearity in the pressure measurement program). Nevertheless, even such a dependence can potentially be calibrated by two quadratic polynomials. Also in the figure, the vertical dotted lines show the refractive coefficients of several gases — helium, neon, argon and carbon dioxide. When performing thermal compensation, it is possible to distinguish between helium and neon.

From the given experimental data, it is possible to estimate the main parameters of this sensor. If we subtract the temperature drift λ_{max} during one letting-to-air cycle at 50 pm, then the full spectral interval of the maximum offset was $\Delta\lambda = 0.3$ nm. Then the sensitivity of this sensor can be estimated in $S_\lambda = \Delta\lambda/\Delta n \approx 1000$ nm/RIU ($\Delta n = 2.9 \cdot 10^{-4}$ RIU). Hence the sensor quality parameter FOM $= 529\,\text{RIU}^{-1}$, with the contrast of the interference pattern $C_R \approx 0.9$. The resolution of δn was estimated by the following method. Approximation polynomials λ^{appr}_{max} of the third degree were calculated for each step Fig. 4, *a* under the assumption that the temperature effect within each step is smooth and monotonous. This polynomial was taken as a systematic part of the error. To calculate the stochastic part of the error, which was taken as an estimate of δn, the standard deviation σ_λ of the difference $\lambda_{max} - \lambda^{appr}_{max}$ was calculated for each step. Among all the values of σ_λ, the smallest was chosen, it was $\sigma^{min}_\lambda = 0.068$ pm. If we correlate this value with $\Delta\lambda$ and Δn, we can get the resolution of this system $\delta n = \Delta n \sigma^{min}_\lambda/\Delta\lambda = 6.5 \cdot 10^{-8}$ RIU.

It is worth noting that the theoretical work [11] describes a sensor made in a diffraction pattern with a signal minimum width of 0.17 nm, which, apparently, is a record value at a sensitivity of 1544 nm/RIU, comparable to the sensor studied in this work. The RI method makes it possible to reduce the spectral width of the signal maximum simply by increasing the number of layers of the multilayer coating of the mirror M_1, i.e. by increasing the FOM sensor, which makes it possible to reduce σ^{min}_λ. To obtain a peak width of about 0.1 nm, two more pairs of layers $(LH)^2$ will be required. Ones can increase $\Delta\lambda$ by increasing the sensitivity when approaching the angle of total internal reflection. Thus, the potential resolution of this sensor can be significantly increased if precision thermal compensation is carried out. The limiting factor of the constant increase in the Q-factor of the resonator may be, in addition to losses in the layers for absorption and scattering, the drift of the beam due to an oblique incidence, which, apparently, will have a significant impact in the fiber version, when the mode size is small in tens of microns. To reduce the drift factor, it is more profitable to use dielectrics with the highest refractive index contrast both in the mirror M_1 and in the base layer, for example, at a wavelength of 1550 nm — Si and SiO_2. However, ultimately it is necessary to take into account the specifics of the application for which the sensor is being

manufactured, in terms of the required thermal sensitivity and chemical resistance.

As the experiment has shown, in order to obtain a maximum in a given spectral range, it is necessary to use optical control in the manufacture of a sensitive layer in order to automatically take into account all the amplitude and phase features of the multilayer structure.

5. Conclusion

The RI method for the oblique incidence of light used to create a sensitive layer of the refractive index sensor in the Kretschmann scheme is experimentally demonstrated. A theoretical description of the sensor parameters is given. It has been experimentally demonstrated that this sensor can have a spectral width of the signal reflection maximum comparable to the reflection spectrum of a fiber Bragg lattice in a single-mode fiber. It has been shown, that the test sample can be used to determine the air pressure up to 10^{-3} bar. When performing thermal compensation, it is possible to distinguish gases close by refractive index, such as helium and neon. The spectral sensitivity was 1000 nm/RIU, the resolution of the sensor in this configuration (without precision thermal compensation) is estimated as $6.5 \cdot 10^{-8}$ RIU and the quality parameter — 529 RIU^{-1}. Proposals for further improvement of the sensor characteristics are formulated.

Funding

The work was supported by the Russian Science Foundation (grant No.21-72-30024). Experimental studies were carried out on the equipment of the Center for Collective Use „Spectroscopy and Optics “ at the Institute of Automation and Electrometry SB RAS.

Conflict of interest

The authors declare that they have no conflict of interest.

References

[1] J. Homola. *Surface Plasmon Resonance Based Sensors* (Springer, 2006). DOI: 10.1007/b100321
[2] J. Jing., K. Liu, J. Jiang, T. Xu, S. Wang, J. Ma, Z. Zhang, W. Zhang, T. Liu. Photon. Res., **10**, 126–147 (2022). DOI: 10.1364/PRJ.439861
[3] M. Printz, J.R. Sambles. J. Modern Optics, **40** (11), 2095 (1993). DOI: 10.1080/09500349314552131
[4] R. Boruah, D. Mohanta, A. Choudhury, G.A. Ahmeda. Opt. Mater., **39**, 273 (2015). DOI: 10.1016/j.optmat.2014.11.014
[5] V.S. Terent'ev, V.A. Simonov. Opt. Spectrosc., **129** (8), 1091 (2021). DOI: 10.1134/S0030400X21080191.
[6] N.D. Goldina. J. Opt. Technol., **89** (2), 71 (2022). DOI: 10.1364/JOT.89.000071
[7] P.F. Egan, J.A. Stone, J.K. Scherschligt, A.H. Harvey. J. Vacuum Sci. Technol. A, **37**, 031603 (2019). DOI: 10.1116/1.5092185
[8] D. Mari, M. Bergoglio, M. Pisani, M. Zucco. Measur. Sci. Technol., **25** (12), 125303 (2014). DOI: 10.1088/0957-0233/25/12/125303
[9] Y. Clergent, C. Durou, M. Laurens. J. Chem. Eng. Data, **44**, 197 (1999). DOI: 10.1021/je980133o
[10] A.D. Kersey, M.A. Davis, H.J. Patrick, M. LeBlanc, K.P. Koo, C.G. Askins, E.J. Friebele. J. Lightwave Technol., **15** (8), 1442 (1997). DOI: 10.1109/50.618377
[11] L. Rahimi, A.A. Askari. Appl. Opt., **59** (34), 10980 (2020). DOI: 10.1364/AO.405129